Reinvestigation of Phase Transitions in $Na_{0.5}Bi_{0.5}TiO_3$ by TEM. Part I: First Order Rhombohedral to Orthorhombic Phase Transition

V. Dorcet,[†] G. Trolliard,*,[†] and P. Boullay[‡]

Laboratoire Sciences des Procédés Céramiques et des Traitements de Surface, SPCTS-CNRS-UMR-6638, 123, Av. Albert Thomas, F-87060-Limoges Cedex, France, and Laboratoire de Cristallographie et Sciences des Matériaux, CRISMAT-UMR 6508 CNRS/ENSICAEN, 6 Bd. du Maréchal Juin, F-14050-Caen Cedex, France

Received February 15, 2008. Revised Manuscript Received June 2, 2008

This study shows for the first time that the rhombohedral to tetragonal phase transition in $Na_{0.5}Bi_{0.5}TiO_3$ (NBT) is a two step phase transition. The transformation begins by a first order phase transition involving the reconstructive transformation of the rhombohedral phase into an orthorhombic one, through the formation of an intermediate modulated phase. This phase transition begins slightly over 200 °C by the disappearance of the ferroelectric−ferroelastic domains. The intermediate modulated phase is then formed from 230 to 300 °C, the temperature at which it disappears. The modulated phase corresponds to an intergrowth of rhombohedral perovskite blocks in which *Pnma* orthorhombic sheets are formed by a microtwinning process of the rhombohedral phase. The intermediate orthorhombic phase is then formed at 300 °C and immediately turns to the tetragonal one. A model is presented explaining the formation of the modulated phase and the origin of the antiferroelectric and relaxor behaviors of NBT.

Introduction

$Na_{0.5}Bi_{0.5}TiO_3$ (NBT) has been thoroughly investigated during the past 40 years mainly for its interesting ferroelectric and dielectric properties. At ambient temperature, this ferroelectric (FE) perovskite compound is rhombohedral (R) with the polar *R*3*c* space group (S.G. No. 161).[1] Temperature in situ studies, carried out by X-ray or neutron diffraction, indicate that two phase transitions occur.[2–6] First, the rhombohedral phase changes to the tetragonal one (T) (*P*4*bm* S.G. No. 100 with $Z = 2$[6]), over a broad temperature range (255−400 °C), during which the two phases coexist.[3–6] According to Vakhrushev et al.[3] this mix of two phases consists of rhombohedral clusters dispersed within a tetragonal matrix that grow as the temperature decreases, until the rhombohedral phase is stable. The cubic (C) prototype form ($Pm\bar{3}m$, S.G. No. 221 with $Z = 1$[6]) appears at about 520 °C, up to the melting point at 1290 °C.[7] This T → C ferroelastic−paraelastic phase transition is well understood. It is of first order, and no temperature hysteresis of the phase transition temperature was observed in heating and cooling of the sample as shown by differential scanning calorimetry experiments (DSC).[8] The temperature of the T → C is also confirmed by optical microscopy studies which show that the twin boundaries characteristic of the ferroelastic tetragonal phase appear near 520 °C during cooling.[9] On the opposite, the R → T phase transition is somewhat questionable as this progressive transformation, which takes place over more than 140 °C,[6] is not in agreement with any kind of mechanisms generally invoked for phase transition.[10]

In a recent review, Isupov[11] has drawn the detailed characteristics of the physical properties of NBT. Concerning the properties, the author emphasized the very good convergence of all the results from the literature. The evolution of the dielectric permittivity versus temperature shows two anomalies related to the two phase transitions arising within NBT.[8,12,13] The curve $\varepsilon'(T)$ shows a frequency dependent small hump at low temperature (ca. 200 °C) exhibiting the relaxor behavior of NBT and a very broad dielectric maximum situated at higher temperature (about 320 °C) that did not depend on the frequency.[13,14] It is also well-known that a ferroelectric (FE)−antiferroelectric (AFE) phase transition occurs near 200 °C,[11–13] that is, roughly the low

* To whom correspondence should be addressed. Tel.: +33 5 55 45 74 94. Fax: +33 5 55 45 72 70. E-mail: gilles.trolliard@unilim.fr.
† SPCTS-CNRS-UMR-6638.
‡ CRISMAT-UMR 6508 CNRS/ENSICAEN.

(1) Vakhrushev, S. B.; Ivanitskii, B. G.; Kvyatkovskii, B. E.; Maisternko, A. N.; Malysheva, R. S.; Okuneva, N. M.; Parfenova, N. N. *Fiz. Tverd. Tela* **1983**, *25*, 2613–2616. (*Sov. Phys. Solid State* **1983**, *25* (9), 1504−1506).
(2) Zvirgzds, J. A.; Kapostins, P. P.; Zvirgzde, J. V.; Kruzina, T. V. *Ferroelectrics* **1982**, *40*, 75–77.
(3) Vakhrushev, S. B.; Isupov, V. A.; Kvyatkovsky, B. E.; Okuneva, N. M.; Pronin, I. P.; Smolensky, G. A.; Syrnikov, P. P. *Ferroelectrics* **1985**, *63*, 153–160.
(4) Suchanicz, J.; Kwapulinski, J. *Ferroelectrics* **1995**, *165*, 249–253.
(5) Kusz, J.; Suchanicz, J.; Böhm, H.; Warczewski, J. *Phase Trans.* **1999**, *70*, 223–229.
(6) Jones, G. O.; Thomas, P. A. *Acta Crystallogr.* **2002**, *B58*, 168–178.
(7) Park, S. E.; Chung, S. J.; Kim, I. T.; Hong, K. S. *J. Am. Ceram. Soc.* **1994**, *77* (10), 2641–2647.
(8) Pronin, I. P.; Syrnikov, P. P.; Isupov, V. A.; Egorov, V. M.; Zaitseva, N. V. *Ferroelectrics* **1980**, *25*, 395–397.
(9) Pronin, I. P.; Syrnikov, P. P.; Isupov, V. A.; Smolenskii, G. A. *Pis'ma v ZhTF* **1982**, *8* (21), 1309–1310. (*Sov. Technol. Phys. Lett.* **1982**, *8* (11), 563−564).
(10) Salje, E. K. H. In *Phase transition in ferroelastic and co-elastic crystals*; Putnis, A., Liebermann, R. C., Eds.; Cambridge University Press: New York, 1990; p 230.
(11) Isupov, V. A. *Ferroelectrics* **2005**, *315*, 123–147.
(12) Sakata, K.; Masuda, Y. *Ferroelectrics* **1974**, *7*, 347–349.
(13) Suchancz, J.; Mercurio, J.-P.; Marchet, P.; Kruzina, T. V. *Phys. Status Solidi B* **2001**, *225* (2), 459–466.
(14) Dorcet, V.; Marchet, P.; Trolliard, G. *J. Eur. Ceram. Soc.* **2007**, *27*, 4371–4374.

10.1021/cm8004634 CCC: $40.75
Published on Web 07/11/2008

temperature anomaly. Above 400 °C, the Curie−Weiss law is fulfilled and NBT is clearly paraelectric (PE).[15] However, the paraelectric phase is stable below this temperature, as the main dielectric anomaly (i.e., about 320 °C) represents the change from the antiferroelectric to the paraelectric behavior.[12,15]

If we compare the temperatures of phase transition, deduced on one hand from the structural studies[2–6] and on the other from the experimental physical properties,[8–15] no clear correspondence exists.

(1) Based on X-ray or neutron diffraction studies, the transformation of the rhombohedral phase seems to begin at 255 °C while the ferroelectric character of the rhombohedral phase vanishes right at 200 °C.[16,17]

(2) From the physical properties, four different phases associated to three phase transitions may arise during the overall temperature sequence, while only three phases and then two phase transitions were evidenced by the structural analyses. All the information mentioned above can be summarized as follows:

		200 °C		**≈320 °C**		**520 °C**	
physical properties	FE (FElast)	→	AFE	→	PE (FElast)	→	PE (PElast)
structural properties	R	→	T + R	→	T	→	C

Then, between 200 and 320 °C, the correlation between the properties and the structure is not yet understood, and in this temperature range, three main points are still under controversy.

(1) The existence of an AFE phase is not confirmed by previous X-ray and neutron diffraction experiments. Indeed, the occurrence of a mix of a ferroelectric (R) and paraelectric (T) phases evidenced by these numerous structural studies does not account for the antiferroelectric behavior of NBT in this temperature range.

(2) This transition between 200 and 320 °C is also associated with a large hysteresis of about 60 °C of different physical properties: thermal,[8] dielectric,[8] optical,[18–20] and mechanical.[21] The structural origin of the temperature hysteresis of the phase transition is not yet explained.

(3) The relaxor behavior of NBT that takes place in this domain of temperature is not fully understood, even if it was suggested by Vakhrushev et al.[3] that the relaxor behavior is due to the occurrence of polar R-clusters dispersed within a nonpolar T-matrix.

In this study we first propose a temperature in situ analysis carried out by transmission electron microscopy (TEM). The comprehensive investigation of NBT by TEM at the ambient temperature has been presented in a previous paper.[22] The aim of this new study is to focus on the first phase transition between 200 and 300 °C, in order to reveal faint structural information either by electron diffraction or conventional imaging. In the discussion, we propose a model accounting for structural changes and explaining the existence of both antiferroelectric and relaxor behaviors in NBT.

Experimental Section

The compound $Na_{0.5}Bi_{0.5}TiO_3$ was prepared by a classical solid state route. Stoichiometric amounts of highly pure reagents (Na_2CO_3, Bi_2O_3, and TiO_2) were mixed and fired at 900 °C for 4 h. Then, after grinding, the obtained powder was sintered at 1120 °C for 1 h. Observations by TEM, carried out both at ambient temperature and during in situ experiments, were performed on a JEOL 2010 microscope operating at 200 kV. A double tilt heating stage was used allowing experiments in the 20 °C−700 °C temperature range. Samples for TEM were prepared by mechanical polishing followed by Ar-ion beam milling. The CaRIne v3.1 software was used to index selected area electron diffraction (SAED) patterns.

Results

NBT crystals show ferroelectric domains which generally present lamellar morphology.[22] In the pseudocubic perovskite subcell, they present interface boundaries lying in both $\{110\}_P$ and $\{100\}_P$ planes.[22] Figure 1 presents the evolution of the microstructure as the temperature raises. All micrographs were obtained in the vicinity of a $\langle 100\rangle_P$ zone axis orientation, and then at the ambient temperature (Figure 1a), the observed $\{100\}_P$ ferroelectric domain walls are viewed edge-on. The ferroelectric domains are about 20 nm thick. They are observed until 200 °C (Figure 1c), the temperature at which they begin to disappear. They have fully disappeared at 230 °C (Figure 1d). In parallel, a fine striation appears, parallel to the interface boundaries of the ferroelectric domains (Figure 1e). This striation then becomes finer and finer as the temperature increases, forming a one-dimensional modulated structure (Figure 2). The Fourier transform calculated from the image obtained at 240 °C shows elongated Bragg reflections at commensurate positions that account for the establishment of this modulated structure (see inset in Figure 2). The reinforcement of intensity is observed at a "q" value of the diffusion vector ranging between 0.018 and 0.022 $Å^{-1}$. The periodicity of the modulation is then about 50 Å. These observations are in fair agreement with the results obtained by Balagurov et al.[23] Indeed, these authors have shown the existence of a one-dimensional modulated structure by in situ neutron diffusion experiments in the same temperature range. The magnitude of the wavelengths invoked in their study was quite similar to the one observed by TEM. The occurrence of such one-dimensional modulated structure is concomitant to the disappearance of the ferroelectric domains and

(15) Pronin, I. P.; Syrnikov, P. P.; Isupov, V. A.; Smolenskii, G. A. *Pis'ma v ZhTF* **1979**, *5* (12), 705–706. (*Sov. Technol. Phys. Lett.* **1979**, *5* (6), 289−290.)
(16) Suchanicz, J.; Ptak, W. S. *Ferroelecrics Letters* **1990**, *12*, 71–78.
(17) Emel'yanov, S. M.; Raevskii, I. P.; Smotrakov, V. G.; Savenko, F. I. *Fiz. Tverd. Tela* **1984**, *26* (6), 1897–1899, Sov. Phys. Solid State, **1984**, 26 (6), 1151−1152.
(18) Isupov, V. A.; Pronin, I. P.; Kruzina, T. V. *Ferroelectr. Lett.* **1984**, *2*, 205–208.
(19) Kruzina, T. V.; Duda, V. M.; Suchanicz, J. *Mater. Sci. Eng.* **2001**, *B87*, 48–52.
(20) Geday, M.; Kreisel, J.; Glazer, A. M.; Roleder, K. *J. Appl. Crystallogr.* **2000**, *33*, 909–914.
(21) Suchanicz, J. *J. Mater. Sci.* **2002**, *37*, 489–491.
(22) Dorcet, V.; Trolliard, G. *Acta Mater.* **2008**, *56* (8), 1753–1761.
(23) Balagurov, A. M.; Koroleva, E. Y.; Naberezhnov, A. A.; Sakhnenko, V. P.; Savenko, B. N.; Ter-Oganessian, N. V.; Vakhrushev, S. B. *Phase Transitions* **2006**, *79* (1−2), 163–173.

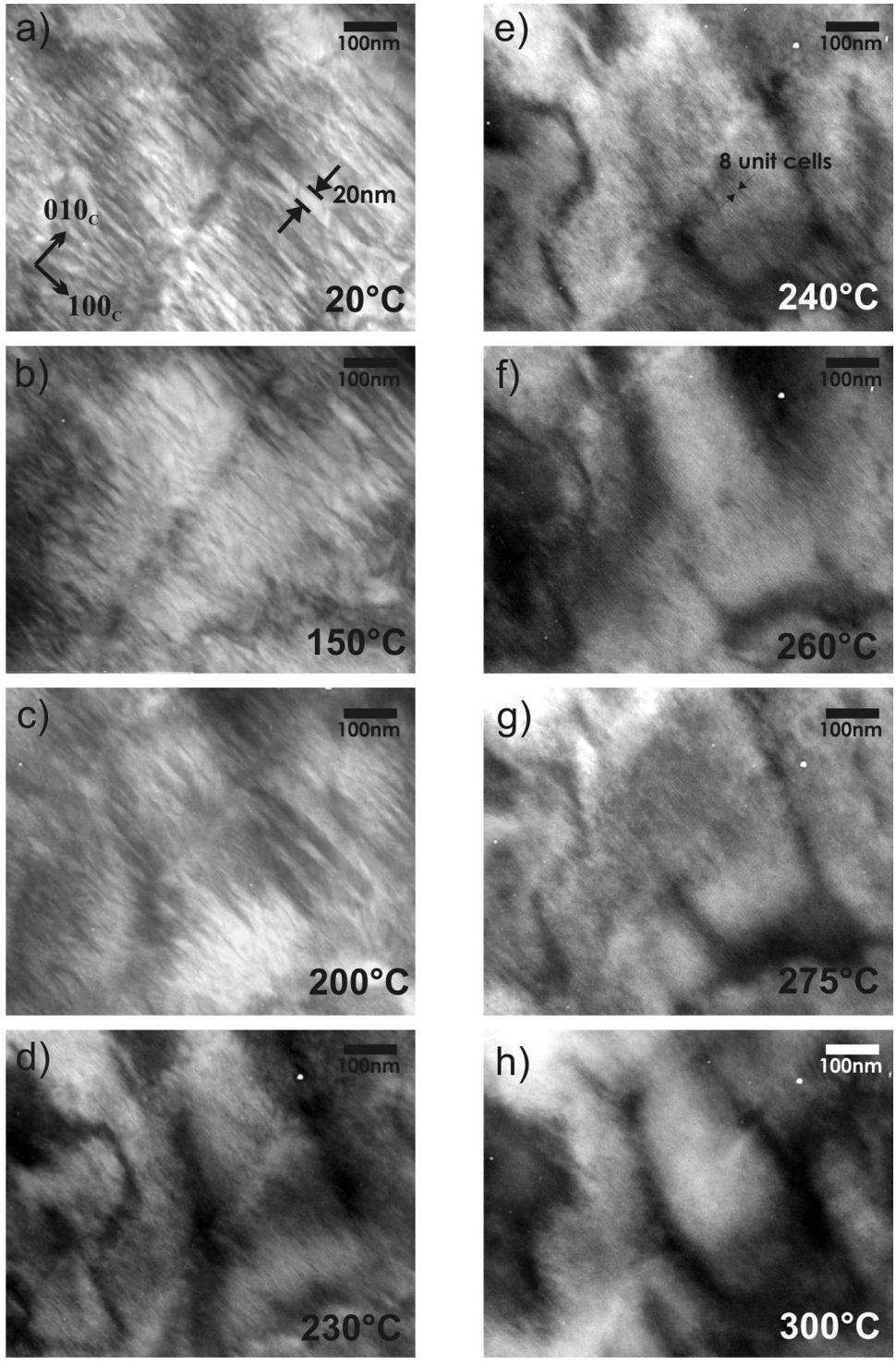

Figure 1. Evolution of the microstructure with the temperature increasing during the in situ experiment. Images are obtained along the $[001]_P$ zone axis pattern. The respective temperatures are reported on the micrographs: (a) 20 °C, (b) 150 °C, (c) 200 °C, (d) 230 °C, (e) 240 °C, (f) 260 °C, (g) 275 °C, and (h) 300 °C.

attests to a phase transition between 200 and 230 °C. This modulated structure is then observed during a large temperature range and disappeared only at 300 °C (Figure 1h).

SAED experiments were carried out in order to understand the origin of such a modulation, arising in NBT between 200 and 300 °C. At first sight, the choice of the most characteristic zone axis pattern (ZAP), under which the two successive phase transitions R → T and T → C will be easily observed, appears as crucial. Indeed, the retained orientation must allow following the evolution of the symmetry of NBT on the overall temperature range. In the study of the ambient form of NBT,[22] it has been shown that the NBT crystals always present $(001)_T$ residual platelets of the high temperature tetragonal phase. Considering, in a first approach, that NBT behaves as an A-site disordered perovskite (R, *R*3*c*; T, *P*4*bm*; and C, $Pm\bar{3}m$ according to ref 6), three types of reflections are then

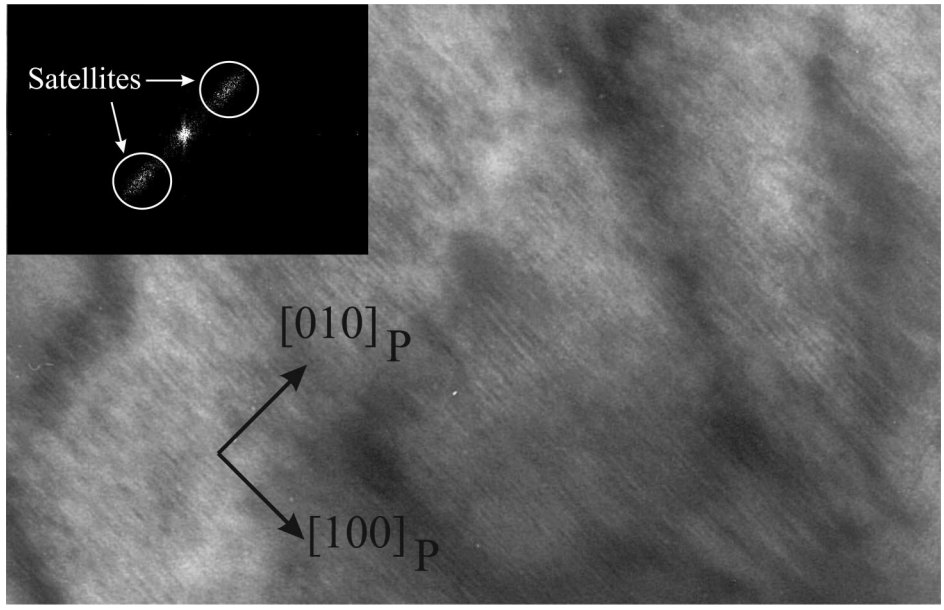

Figure 2. Observation of the modulated structure at 240 °C. The 1024 × 1024 Fourier transform is shown on the inset.

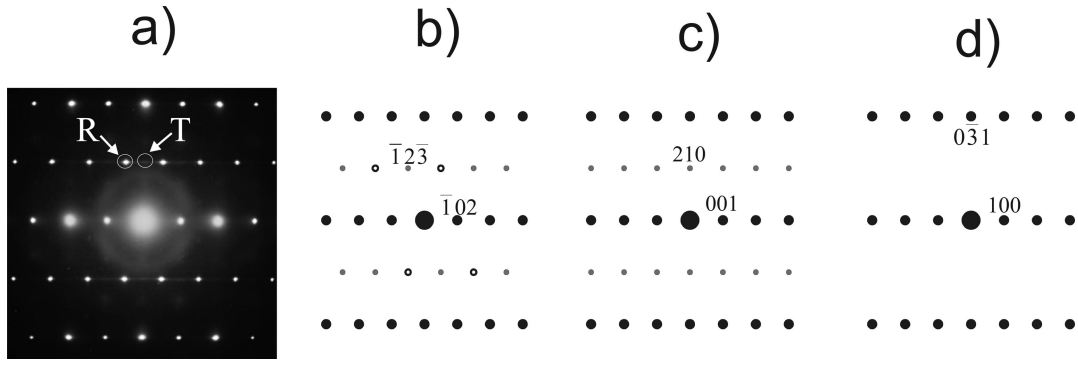

Figure 3. Comparison between the experimental $[013]_P$ SAED pattern with different simulations. (a) Experimental diagram. (b) Geometrical simulation for the *R*3*c* rhombohedral cell. The cubic sublattice is represented by large dark dots while rhombohedral superstructure spots are represented by small gray dots. Extinctions are reported as open circles. (c) Geometrical simulation for the *P*4*bm* tetragonal cell. The cubic sublattice is represented by large dark dots while tetragonal superstructure spots are represented by small gray dots. (d) Geometrical simulation for the $Pm\bar{3}m$ cubic cell.

observed in the electron diffraction patterns: (1) the fundamental reflections characteristic of the pseudocubic sublattice of the perovskite, (2) $^1/_2(ooo)$ superstructure reflections (where *o* represents odd values of the Millers indices) typical of the rhombohedral supercell and induced by the $a^-a^-a^-$ octahedral tilting system of the rhombohedral phase, and (3) $^1/_2(ooe)$ superstructure reflection (where *e* represents an even value of the Millers indices) due to the $a^0a^0c^+$ in-phase tilting system of the tetragonal platelets. These reflections are typically elongated along $[100]^*_P$ as a consequence of the restricted thickness of the platelets, which are only a few cells thick.[22]

In addition, these experimental patterns also present characteristic diffuse streak lines parallel to $[100]^*_P$. Their presence was attributed to an aperiodic distribution of the tetragonal platelets within the rhombohedral phase.[22]

Figure 3 shows that the $[013]_P$ zone axis pattern is well appropriated for this in situ temperature study. Under this orientation the experimental pattern observed at the ambient temperature (Figure 3a) displays the $^1/_2(ooo)$ superstructure reflections (R type) from the rhombohedral phase (see Figure 3b) as well as the elongated tiny $^1/_2(ooe)$ reflections (T type) due the tetragonal platelets (see Figure 3c). Therefore, the evolution of the respective intensity of these reflections seems a good criterion to observe the first R → T phase transition. It is also shown that the second phase transition T → C will theoretically lead to the disappearance of both $^1/_2(ooo)$ and $^1/_2(ooe)$ reflections and that, in such a case, only the sublattice reflections of the cubic cell will be finally observed (Figure 3d). This ZAP also allows the evolution of the intensity of the diffuse streak lines parallel to $[100]^*_P$ to be followed.

Figure 4 represents different SAED patterns obtained at different temperatures under the $[013]_P$ zone axis. The main results are the following.

(1) As the temperature rises, the intensity of the $^1/_2(ooo)$ (R) reflections progressively decreases while that of the $^1/_2(ooe)$ (T) increases until 400 °C (Figure 4e).

(2) The elongation of the $^1/_2(ooe)$ (T) reflections, which characterizes the tetragonal platelets, persists up to 400 °C (Figure 4e) and removes above (Figure 4f). This clearly means that the tetragonal platelets do not act as preferential nucleation sites in the R → T phase transition, at least not below this temperature.

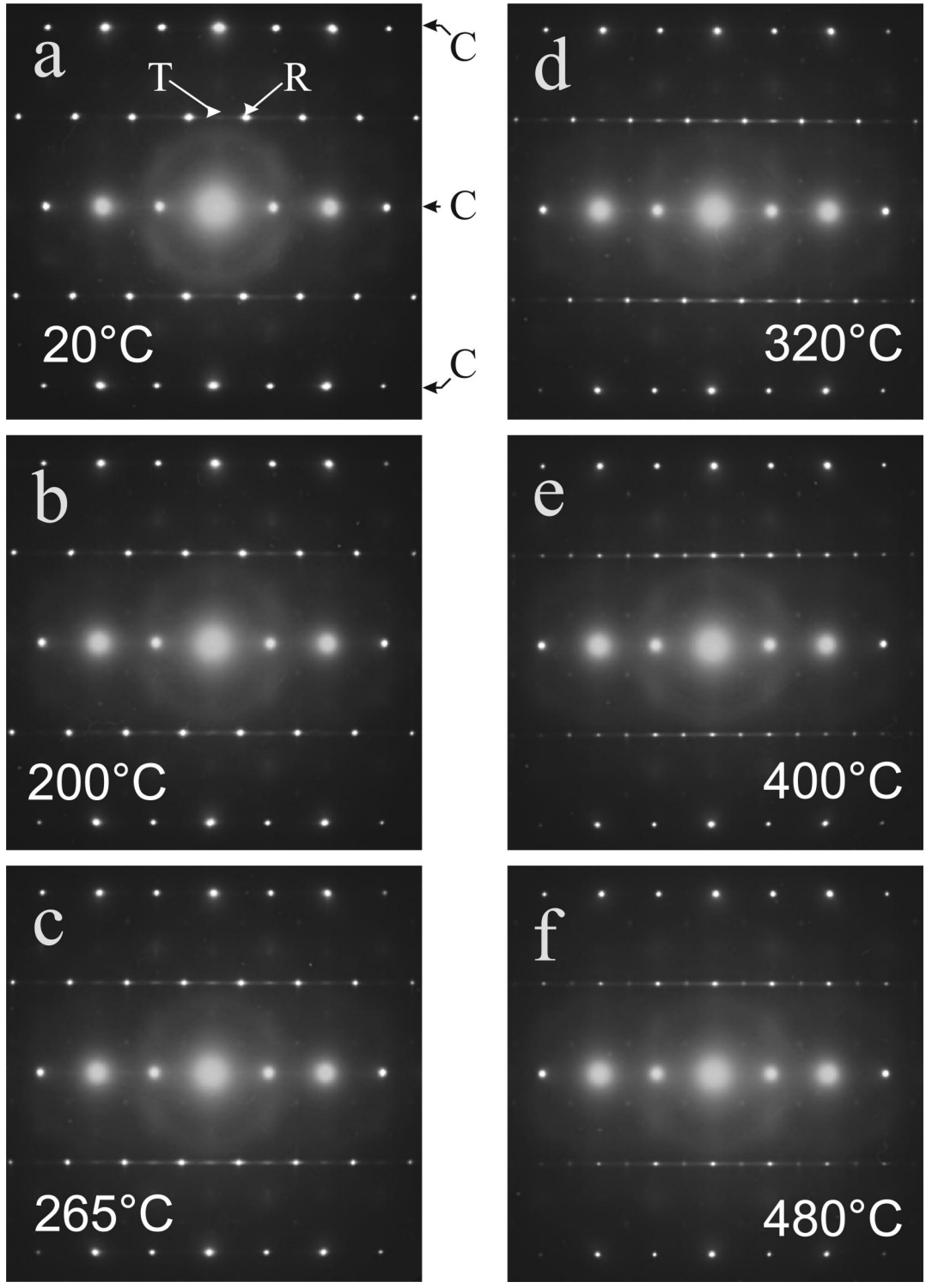

Figure 4. Evolution of the $[013]_P$ SAED pattern with the temperature increasing during the in situ experiment. The $^1/_2(ooo)$ reflections are labeled R while $^1/_2(ooe)$ spots are labeled T. The C reflections are common to both rhombohedral and tetragonal cells and also represent the cubic cell. The respective temperatures are reported on the micrographs: (a) 20 °C, (b) 200 °C, (c) 265 °C, (d) 320 °C, (e) 400 °C, and (f) 480 °C.

The evolution was then considered under the $[111]_P$ ZAP (Figure 5). This orientation allows the superstructure diffraction spots $^1/_2(ooe)$ of the three variants of the tetragonal platelets to be observed,[22] namely, T1, T2, and T3 in Figure 5e. All of these reflections are seen whatever the temperature. This experiment also corroborates the results obtained with the $[013]_P$ ZAP as these T reflections remain elongated until 320 °C (Figure 5d) in spite of the their progressive increase in intensity. They only became punctual at 480 °C (Figures 4f and 5f). It is thus concluded that the phase transition which begins at 200 °C does not correspond to the growth of the tetragonal platelets. The nature of the first phase transition leading to the disappearance of the ferroelectric−ferroelastic domains near 200−230 °C was revealed by SAED observations in the vicinity of a $[001]_P$ zone axis patterns. Indeed, Figure 6 shows that at 300 °C, some new $^1/_2(oee)$ superstructure reflections are present. They are no longer visible at 400 °C but reappear during the cooling, in the same

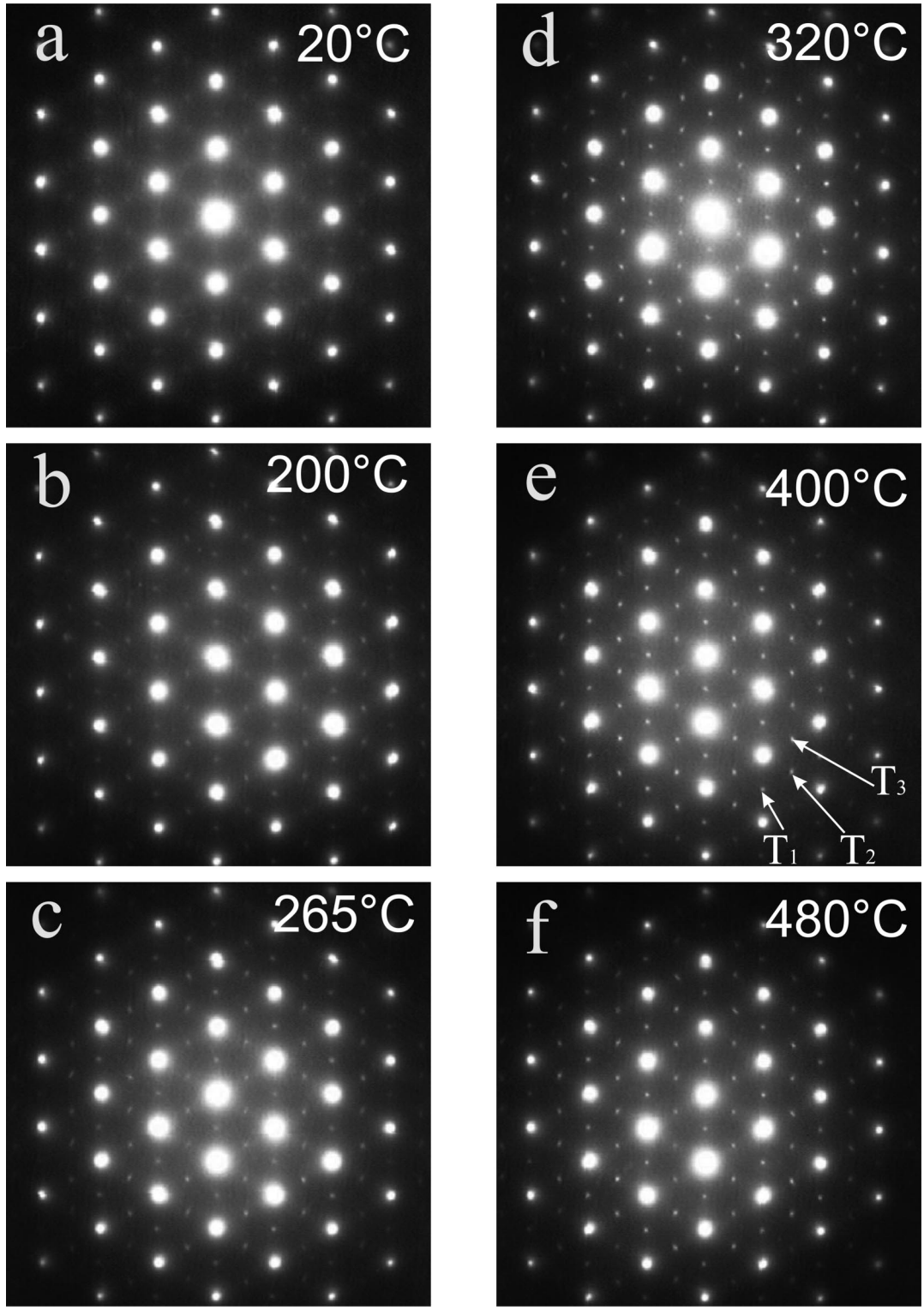

Figure 5. Evolution of the intensity of the $^1/_2(ooe)$ reflections of the three tetragonal variants in the $[111]_P$ SAED pattern with the temperature increasing. The respective temperatures are reported on the micrographs: (a) 20 °C, (b) 200 °C, (c) 265 °C, (d) 320 °C, (e) 400 °C, and (f) 480 °C.

domain of temperature (Figure 6). These new $^1/_2(oee)$ superstructure reflections strongly suggest that a new phase is formed between the rhombohedral and the tetragonal phases. Figure 6 attests that the formation of this new phase is reversible. A supplementary electron diffraction experiment was then carried out in order to determine more precisely the domain of temperature of this new phase (Figure 7). The overall pattern of the zero order Laue zone, situated in the upper part of Figure 7, shows that the $^1/_2(oee)$ reflections are better seen under slightly tilted ZAP conditions. A series of enlargements is provided below. These superstructure spots appear at 200 °C and are still visible at 320 °C. They then disappeared in the 320−370 °C temperature range. These new reflections could not be indexed by the different space groups previously proposed in the literature ($R3c$,[1] $P4bm$,[6] $P4_2nm$[24]), and more generally, they could not be

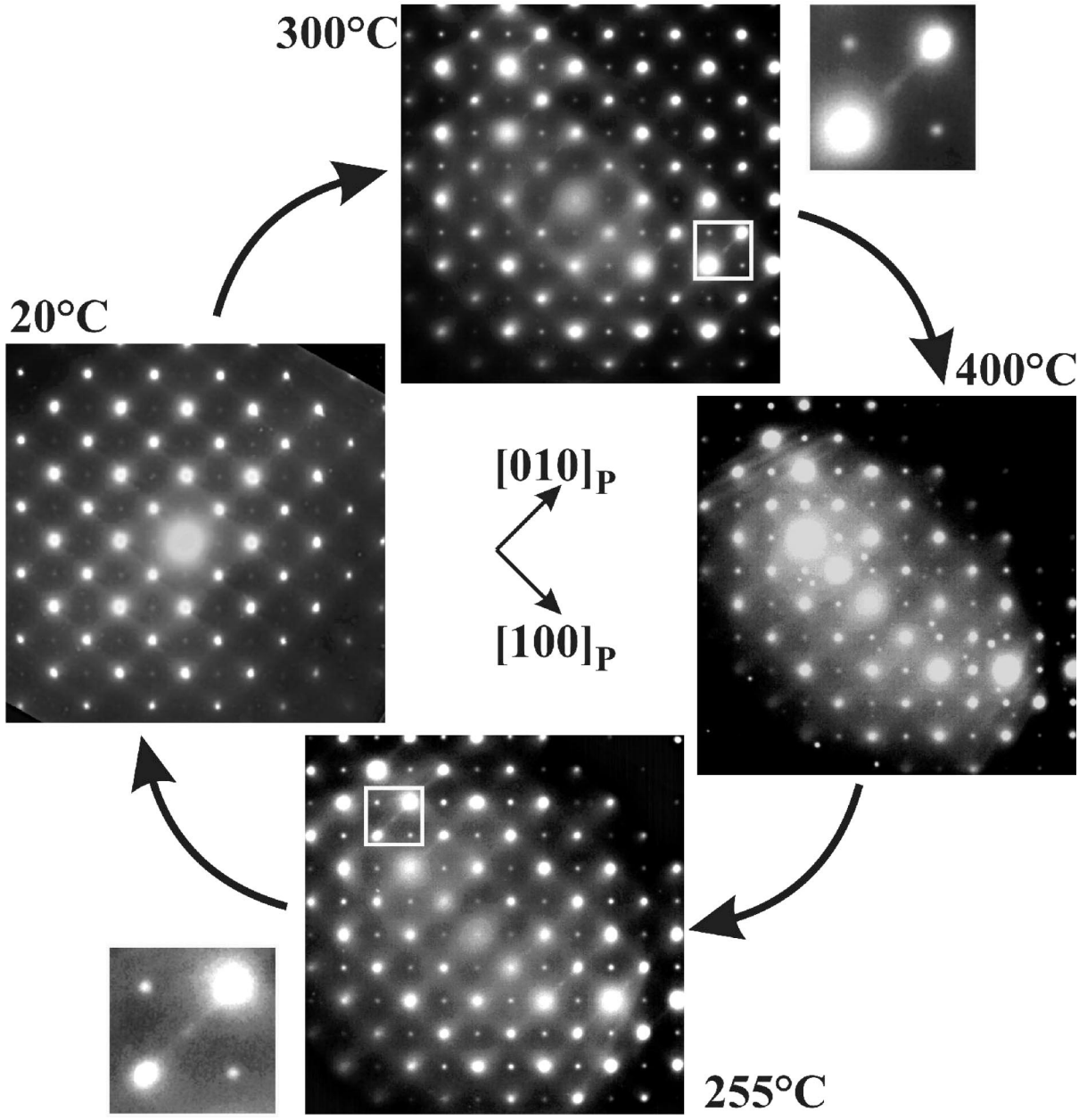

Figure 6. In situ observation along the $[001]_P$ zone axis pattern showing the appearance of $^1/_2(oee)$ reflections characteristic of an orthorhombic phase. The upper and lower parts of the figure respectively report the results obtained during the temperature increases and decreases, showing a reversible character of the transformation.

indexed by a tetragonal phase and attest of a symmetry lowering. An orthorhombic symmetry can be deduced, considering the different SAED patterns obtained at that temperature. The nature of this new phase will be discussed further on. Finally, it should be noticed that whatever the temperature, theses superstructure spots are elongated parallel to $[100]^*_P$. In addition, diffuse streak lines has appeared parallel to $[100]^*_P$, passing through these $^1/_2(oee)$ reflections. This new phase thus appears under the form of platelets, or perovskite sheets, developed in the $\{100\}_P$ planes of the pseudocubic cell.

Discussion

Three main points will be respectively discussed. The first one concerns the evolution of the crystalline symmetry of NBT against the temperature and the structural reasons that lead to the formation of the new phase. The second part of the discussion will present a model explaining the formation of the modulated structure, and the last part of the discussion will be devoted to the correlation existing between this structural evolution and the physical properties known from the literature. A specific consideration will be paid on the explanation of the origin of these so-called antiferroelectric and relaxor behaviors of NBT observed in the 200−300 °C temperature range.

1. First Phase Transition Encountered between 200 and 300 °C. All the in situ structural studies dealing with phase transition of NBT agreed with the fact that no structural evolution is evidenced below 255 °C.[4–6] However, in the

(24) Petzelt, J.; Khamba, S.; Fabry, J.; Noujni, D.; Porokhonskyy, V.; Pashkin, A.; Franke, I.; Roleder, K.; Suchanicz, J.; Klein, R.; Kugel, G. E. *J. Phys.: Condens. Matter* **2004**, *16*, 2719–2731.

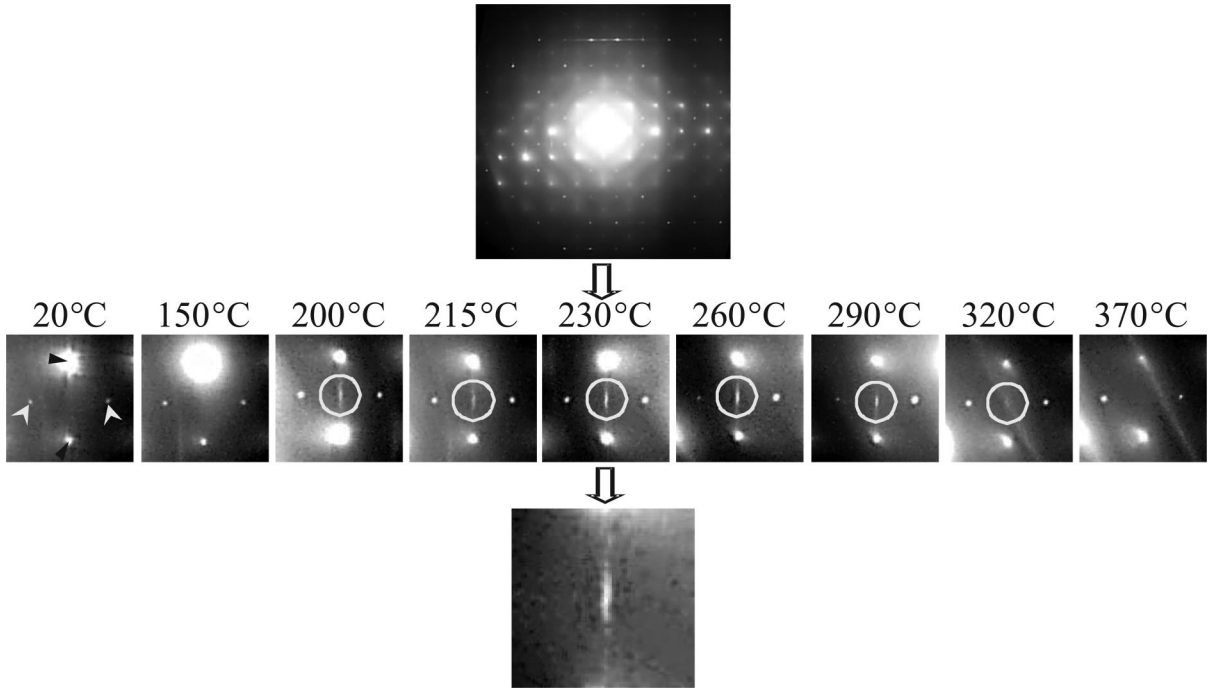

Figure 7. Comprehensive in situ study between 20 and 370 °C carried out near the $[001]_P$ zone axis pattern direction. It shows the stability temperature range of the orthorhombic phase. A series of enlargements is provided for the different investigated temperatures. On the first of them (at 20 °C) the black arrows indicate the cubic sublattice reflections while the white ones indicate the position of the $^1/_2(ooe)$ tetragonal reflections. The $^1/_2(oee)$ reflections characteristic of an orthorhombic phase are encircled when present.

present study, the [001] ZAP electron diffraction patterns show the appearance of a new $^1/_2(oee)$ superstructure spots right from 200 °C. Their intensity is then gradually reinforced up to 300 °C before decreasing until being zero above 320 °C (Figure 7). In addition, the ferroelectric domains disappeared since 200 °C (Figure 1 c,d), meaning that the rhombohedral phase began to transform at that temperature. This disappearance is concomitant with the formation of a modulated structure (Figure 2) displaying a long-range ordering tendency. These $^1/_2(oee)$ reflections are stretched along a direction parallel to that of the modulation, that is, $\langle 100\rangle_P$.

This modulated texture testifies a first order phase transition involving a reconstructive transformation process.[10,25] It may be described using a 3+1D formalism like any modulated phase.[26] This phase presents a 3D sublattice linked to the basic periodicities of the perovskite lattice, bearing a one-dimensional modulation along $\langle 100\rangle_P$. One must recall that the periodicity of such modulation is in fair agreement with that recently evidenced by Balagurov et al. by neutron scattering[23] in the same temperature range. Considering that neither neutron[6] nor X-ray diffraction[5] have detected any structure change near 200 °C, the sublattice of the modulated phase should be built up upon the rhombohedral low temperature phase. The modulation may then be interpreted as a more or less periodic distribution of orthorhombic perovskite sheets, with their own octahedra tilting system, developed as an intergrowth within the rhombohedral matrix, as shown by the stretching of the $^1/_2(oee)$ reflections and by the existence of diffuse streak lines parallel to $[100]^*_P$. The symmetry of this new phase is strongly influenced by the rhombohedral host matrix, and the determination of the octahedral tilting condition must meet these two criteria:

(1) According to the work of Woodward et al.[27] the presence of $^1/_2(oee)$ superstructure reflections within pseudocubic perovskites may only be relevant to a combination of in-phase and antiphase octahedra tilting systems. Only four possible systems may then be invoked: $a^+a^+c^-$ ($I4_2/nmc$), $a^0b^+c^-$ ($Cmcm$), $a^-b^+a^-$ ($Pnma$), and $a^+b^-c^-$ ($P2_1/m$).

(2) Given that the average structure is mainly disordered, the only possibility of tilting systems allowing an A-site as unique are as following: $a^0a^0a^0$, $a^0a^0c^+$, $a^0a^0c^-$, $a^0b^-b^-$, $a^-a^-a^-$, and $a^-b^+a^-$.[28]

Only the $a^-b^+a^-$ system meets these two conditions. It corresponds to the *Pnma* space group. The modulated phase will then consist in a rhombohedral matrix in which orthorhombic sheets of perovskite will form with increasing temperature. Owing to the $a^-b^+a^-$ tilting system, the relation between the orthorhombic phase and the prototype cubic phase is thus as follows: $a_O \approx a_p\sqrt{2}$, $b_O \approx 2a_p$, and $c_O \approx a_p\sqrt{2}$. The formation of an orthorhombic phase is certainly not fortuitous.

(1) *Pnma* is the most commonly encountered space group in perovskite compounds.[29]

(25) Blinc, R.; Levanyuk, A. P. Incommensurate phases in dielectrics. In *Modern problems in condensed matter sciences*; Agranovich, V. M., Maradudin, A. A., Eds.; North-Holland Physics Publishing: New York, 1986; Vol. 14.1.
(26) Janssen, T.; Janner, A.; Looijenga-Vos, A.; de Wolff, P. M. In *International Tables for Crystallography*, 2nd ed.; Wilson, A. J. C., Prince, E., Eds.; Kluwer Academic Publishers: Norwell, MA, 1999; Vol. C, Chapter 9.8.
(27) Woodward, D. I.; Reaney, I. M. *Acta Crystallogr.* **2005**, *B61*, 387–399.
(28) Woodward, P. M. *Acta Crystallogr.* **1997**, *B53*, 44–66.
(29) Mitchell, R. H. *Perovskites: modern and ancient*; Almaz Press: Thunder Bay, Ontario, 2002.

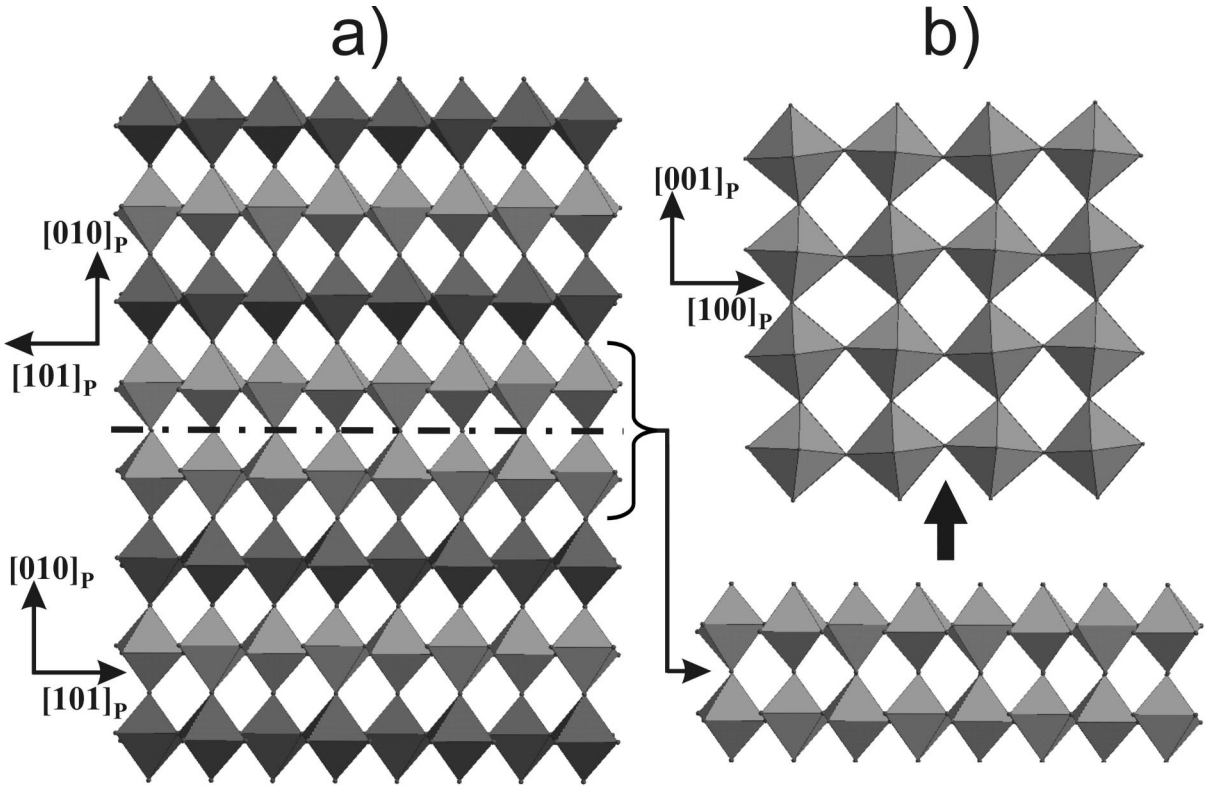

Figure 8. Crystallographic model of pseudomerohedral $\{100\}_P$ twin boundaries of the ferroelectric domains. (a) Projection of the rhombohedral structure viewed along the $[10\bar{1}]_P$ direction. The dashed line represents the position of the $(010)_P$ twin plane. Each domain represents alternating layers in which octahedra are tilted in an obverse (bright octahedra layers) or reverse way (dark octahedra layers). (b) The two octahedra layers situated on each part of the twin boundary are extracted from the model. The in-phase tilting of the two octahedra layers observed both on the $[010]_P$ (upper part) and $[10\bar{1}]_P$ (lower part) projections correspond to $a^-a^+a^-$ tilting system, that is, to a *Pnma* structure.

(2) It corresponds to the high pressure phase of NBT.[30]

(3) There is a group to subgroup relationship with the high temperature tetragonal phase.

In fact, the formation of *Pnma* sheets is easily achieved as it represents natural $\{100\}_P$ twin planes separating two *R*3*c* ferroelectric domains related by a pseudomerohedral twinning law. This is shown in Figure 8, which represents $a^-a^-a^-$ rhombohedral domains with alternating octahedra layers tilted in an obverse and reverse sense (bright or dark layers in Figure 8a). On each side of the interface plane, the two octahedra layers present an in-phase tilting condition corresponding to the $a^-a^+a^-$ tilt system, which is a particular case of the general form $a^-b^+a^-$ generally adopted within orthorhombic crystals. The structural particularity of the $a^-a^+a^-$ orthorhombic phase is then imposed by its structural relationships with the $a^-a^-a^-$ rhombohedral matrix. Indeed, the orthorhombic cell must present an equivalent octahedra tilting rotation angle around the three cubic directions to fit the rhombohedral cell. Between 200 and 300 °C, the twin plane defects represent a preferential nucleation site for the orthorhombic phase. The nucleation and the multiplication of these twin boundaries arise by a microtwining process taking place within the rhombohedral crystal. It finally gives rise to the modulated phase in which the long-range periodicity corresponds to the average distribution of the twin planes, that is, of the orthorhombic sheets, within the *R*3*c* matrix. The establishment of the periodicity may correspond to the minimization of the elastic strain within the crystal. Of course, the diffuse streak lines that appeared parallel to $[100]_P^*$ and passing through the $^1/_2(oee)$ superstructure spots are due to the fact that the long-range periodicity of the modulated phase is not strictly established.

The orthorhombic intermediate phase was however not detected in previous X-ray or neutron experiments. In fact, due to the strong structural analogy arising between the rhombohedral and the orthorhombic structures, the simulation of their respective X-ray patterns shows that such orthorhombic structure is almost undetectable. In addition, and more particularly concerning the neutrons, the more plausible explanation can be the very small size of the regions from which this superstructure originates.

At 300 °C, the modulated phase has disappeared (Figure 1h). However, the $^1/_2(oee)$ superstructure reflections are still present at 300 °C (Figure 6) and even slightly above at 320 °C (Figure 7). It means that near this temperature (280−300 °C) the modulated phase evolves through the orthorhombic phase which is now free to adopt a more general $a^-b^+a^-$ tilt system. This transformation is certainly concomitant to a large strain release and corresponds either to the exothermic anomaly ($T = 304$ °C[18]) observed during temperature increase of DSC experiments or to the "isotropization" point ($T = 290$ °C [18,19]) noticed during optical microscopy studies. Even if the rhombohedral to orthorhombic phase transformation is reversible (Figure 6) the formation of an intermediate modulated structure between these two phases explains the hysteresis effects of about 60 °C

(30) Kreisel, J.; Glazer, A. M.; Bouvier, P.; Lucazeau, G. *Phys. Rev. B* **2001**, *63*, 174106.

observed for different physical properties (see Introduction). Indeed, such thermal hysteresis is generally observed in modulated incommensurate phases.[25]

2. Why an Intermediate Modulated Phase Forms during the R → O Phase Transition. The term "modulated phase" is used by similarity with the long period structures observed for instance in hexagonal perovskites[31] or Aurivillius phases.[32,33] In the 3+1D approach, these phases are treated as commensurately modulated layered structures derived from the perovskite and having the general formula $AB_{1-x}O_3$. The modulation is then related to the periodic distribution of B-cation vacant octahedra layers, which are described as a consequence of crystallographic shears taking place within the perovskite structure. Compared to those compounds, the orthorhombic perovskite sheets of two octahedra layers thick and the twin planes are respectively the structural analogues of the vacant octahedra layers and shearing planes. The rhombohedral phase is thus periodically disturbed by twin planes separating two rhombohedral blocks of the same thickness on each side of it. The modulation wavelength depends on the density of twin planes, that is, of the thickness of the *R*3*c* blocks. However, compared to more conventional long-range ordered perovskites, the formation of twin planes is not accompanied by any chemical change and the modulated phase better corresponds to a strain modulation rather than to a compositional modulation. It is worth noting that the modulation may not originate from compositional fluctuations relying on Na−Bi segregation. Such a phenomenon is in fact impossible or strictly restricted due to the contrasting valence of the two involved cations (+1 for Na and +3 for Bi). The strain modulation is induced by the occurrence of different octahedra tilting conditions within a single crystalline network. From a phenomenological point of view, these strains result from the concomitance of two incompatible order parameters which give rise to the two phases involved in the modulated structure.

(1) A ferroelastic order parameter (F1) is responsible for the ferroelastic C → T phase transition. It prevails within the high temperature tetragonal form and leads to an in-phase rotation $a^0a^0c^+$ of octahedra along the 4-fold axis of the tetragonal cell.

(2) A ferroelastic/ferroelectric order parameter (F2) is responsible for the T → R phase transition, prevailing at low temperature and leading to an antiphase rotation $a^-a^-a^-$ of the octahedra along the threefold axis of the rhombohedral cell and to correlated atomic displacements of cations along the same direction.

In fact the competition between these two order parameters as the temperature decreases gives rise to an intermediate orthorhombic phase in which both in-phase and antiphase tilting systems are observed and in which, consequently, the cation displacement will take place in an intermediate direction, as will be seen later on.

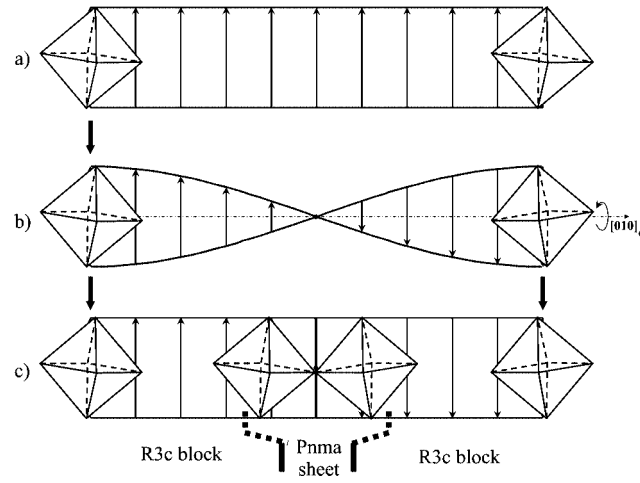

Figure 9. Schematic representation showing the effect of a rotation of 180° applied to a crystal around b_O. In this purely theoretical model, the driving force leading to the modulation is a torsion strain. Each of the two isolated parts of a crystal is symbolized by an octahedron. (a) The initial state within the *R*3*c* crystal. No torsion is applied and all crystallographic directions symbolized by arrows remain constant. The chosen direction is arbitrary. (b) A torsion involving a crystalline rotation of 180° is applied. The involved strain between the two crystal parts is progressively accommodated by slight elementary rotation of each octahedron. The lattice strain propagates within the overall crystal, and this feature case is not energetically favorable and therefore structurally unrealistic. (c) A torsion involving a crystalline rotation of 180° is applied, but in this case the overall lattice strain is abruptly accommodated within a single plane. The strain is localized and minimized within a twin plane.

The structural model that will be developed aims to illustrate the driving force involved in the formation of the modulated phase. In this model, we considered that such driving force is a strain corresponding to a torsion that allows the microtwinning process to occur around the direction of the modulation (Figure 9). Starting from the low temperature rhombohedral phase in which the F2 order parameter predominates, an increase in temperature results in an increase of the torsion, that is, an increase of the influence of F1. Figure 9 represents two separated crystal parts, each of them being symbolized by single octahedron. Starting from a nondistorted crystal (Figure 9a), the application of a torsion induces a tilt of 180° (Figure 9b,c), and the strain relaxation between the two crystal parts may be accommodated in two distinct ways.

(1) In Figure 9b, the strain is accommodated step by step, involving a small value of tilt of each octahedron. The lattice strain propagates within the overall crystal, and this feature case is not energetically favorable as it may involve high elastic strain within the crystal. Furthermore, this model is also structurally unrealistic.

(2) It is also possible that the strain is abruptly accommodated (Figure 9c) by a direct rotation of 180° between two successive octahedra. The strain is then localized and minimized within a twin plane. This configuration is that presented in Figure 8 and is coherent within a microtwinning process.

The latter case then corresponds to the formation of a *Pnma* twin boundary after an operation of a pseudomerohedral twinning law. In this case the two octahedra form a free strain energy interface, and so the nucleation of *Pnma* perovskite sheets within the rhombohedral matrix allow

(31) Boullay, P.; Teneze, N.; Trolliard, G.; Mercurio, D.; Perez Mato, J. M. *J. Solid State Chem.* **2003**, *174*, 209–220.
(32) Boullay, P.; Trolliard, G.; Mercurio, D.; Perez Mato, J. M.; Elcoro, L. *J. Solid State Chem.* **2002**, *164*, 252–260.
(33) Boullay, P.; Trolliard, G.; Mercurio, D.; Perez Mato, J. M.; Elcoro, L. *J. Solid State Chem.* **2002**, *164*, 261–271.

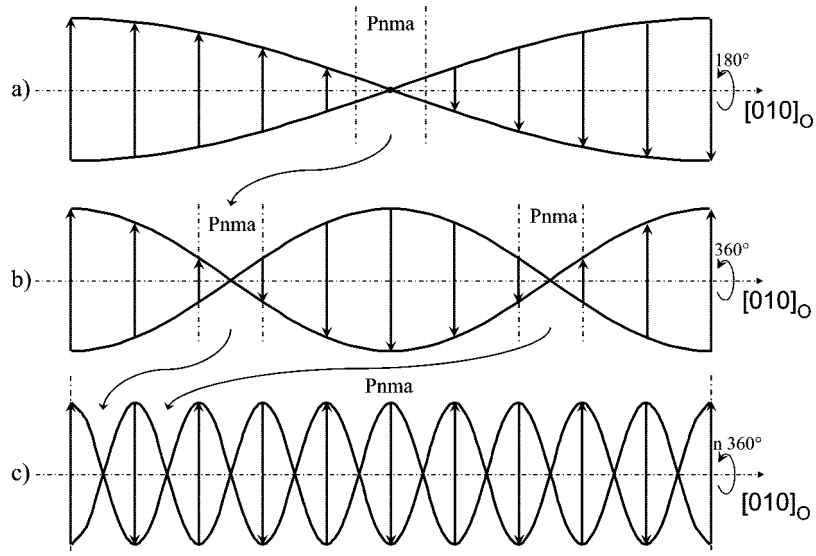

Figure 10. Schematic representation showing that an increase in the torsion strain applied to the crystal, from a to c, results in an increase in the number of *Pnma* perovskite sheets, i.e., an increase in the twin plane density until they fully invade the crystal (c).

accommodating the torsion strain. As the temperature increases, the influence of the order parameter F1 is more sustained, and correlatively the number of *Pnma* perovskite interfaces increases to accommodate the strain (Figure 10), until they invade the overall crystalline space (Figure 10c). The crystal symmetry is then orthorhombic with the *Pnma* space group.

3. Contribution of the Structural Model to the Comprehension of the Electric Properties. NBT shows an antiferroelectric behavior between 200 and 300 °C, and thus, in the crystal, the cations are moved from the center of their polyhedra. The modulated structure arises in the same temperature domain and, for this reason, is clearly associated to this property. Consequently, the direction of the cationic movement is obviously linked to the direction of the modulation. Moving from the low temperature $a^-a^-a^-$ tilt system (R) to $a^-a^+a^-$, the $x0z$ plane of the twin boundary is maintained (Figure 8) and the direction of the modulation consequently stands along the $[010]_O$ direction of the orthorhombic phase. In this case, the direction of the dipolar vectors must turn around b_O (Figure 11). Three main cases have then to be considered.

(1) All cationic displacements are along $[010]_O$ and the polar vectors are orientated along b_O (Figure 11a). In this case the modulation does not have any influence on the polar character of the crystal. The cationic displacements are modulated along this direction and the polar moments as well. The crystal presents a ferroelectric polar character.

(2) The dipolar vectors can take any random orientation (Figure 11b). In this case a polar component exists along the three axis of the orthorhombic cell: a_O, b_O, and c_O. Due to the modulation, the component along a_O and c_O became zero ($\sum\mu_\perp = 0$) while those along b_O are added. The crystal thus presents a ferroelectric or "canted" ferroelectric character.

(3) The cationic displacement takes place solely along a direction perpendicular to b_O (Figure 11c), that is, along a general $[u0w]_P$ direction. The sum of the moment over a period of modulation is zero. The crystal does not behave as a ferroelectric but presents an antiferroelectric character.

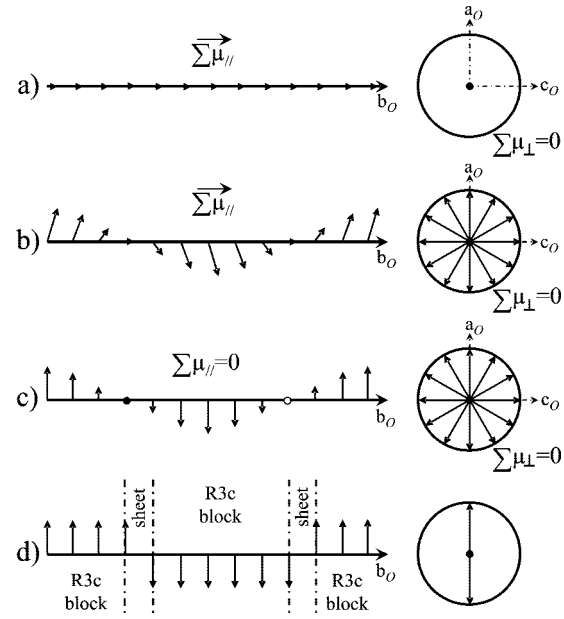

Figure 11. Schematic representation explaining the relation between the orientation of the polar vectors within the modulated phase and its macroscopic electric property. The direction of the moments turns along a screw axis (modulation of direction), and depending on the orientation of the moment with regard to the orthorhombic b_O direction (screw axis), different situations have to be considered. (a) If the cationic displacement occurs along the b_O direction, the polar vectors are added, $\sum\mu_{||} \neq 0$ and $\sum\mu_\perp = 0$, and the crystal is polar. (b) If the moments are directed along an $[u0w]_P$ orientation, then the components along the b_O direction are summed up ($\sum\mu_{||} \neq 0$), while those along any perpendicular direction are canceled ($\sum\mu_\perp = 0$) due to the modulation. The crystal is still polar. (c) If the direction of the moments is perpendicular to the orthorhombic b_O direction, i.e., along a $[u0w]_P$ direction, the sum of the components along b_O is zero ($\sum\mu_{||} = 0$) as well as normal to b_O ($\sum\mu_\perp = 0$). The crystal is antiferroelectric. (d) If the moments are directed perpendicular to the orthorhombic b_O direction but only turn abruptly 180° when they meet a twin plane (*Pnma* sheet), the sum of the components along b_O is zero ($\sum\mu_{||} = 0$) as well as along normal directions ($\sum\mu_\perp = 0$). The crystal is antiferroelectric.

Over the three possibilities presented above, only the last one accounts for the antiferroelectric character evidenced within NBT. It is then concluded that, in the modulated phase, the direction of the polar moments is perpendicular to b_O, that is, along a $[u0w]_P$ direction. In the schematic

representation proposed in Figure 11c the amplitude of the cationic displacement is constant, but from one cationic site to the other its orientation turns continuously around b_O. In this theoretical model, the *u* and *w* values change continuously. In fact, within the crystal lattice, the tilting values of the octahedra are determined within a given structure (*R*3*c* and/or *Pnma*) and the associated cationic displacement as well. It has been shown that the modulated phase is formed by $a^-a^-a^-$ rhombohedral perovskite blocks separated by $a^-a^+a^-$ orthorhombic perovskite sheets (Figure 8). In each perovskite layer, the tilt system is constant, and then within a single block, the *u* and *w* values within each pseudocubic cell are constant too. The moduli of the dipolar moment are then constant, but their sign changes from one block to the next when passing the twinning plane (Figure 11d). This inversion in the sign of the polar vectors from one block to the other is responsible for the antiferroelectric behavior of NBT. This schematic representation (Figure 11d) suggests the existence of layers of a few perovskite cells thick, so that in every layer, the internal deformation resulting in the unit cell dipoles corresponds to *homogeneous* deformation. Therefore, the macro-polarization thus produced is homogeneous polarization. In the modulated phase, the atomic displacements perpendicular to the modulation direction are then described, to a first approximation, using a crenel function. It is worth noting that the internal deformation of the units may also correspond to *heterogeneous* deformation (sine curve or sawtooth functions). Indeed, such cationic distribution may also explain the antiferroelectric behavior. However, we opted for homogeneous deformation as the octahedra tilting is homogeneous within each perovskite block and that such tilting may influence the cationic displacement because the cationic movements are sensitive to the oxygen positions.

However, one should keep in mind that the result is valuable only if the cation displacement is perpendicular to b_O (Figure 11d), that is, along $[u0w]_P$, which was not initially the case within the *R*3*c* structure in which the cationic displacement is along $[111]_P$. Thus, the polar vectors must be reorientated within the *R*3*c* blocks during the transition from the rhombohedral to the modulated phase.

The temperature interval during which the ferroelectric property of the rhombohedral NBT change to the antiferroelectric property of the modulated phase is situated between 200 °C, the temperature at which the ferroelectric domains began disappearing (Figure 1c,d), and 230 °C, temperature of the formation of the modulated phase (Figure 1 d,e; see also refs 11–13). The reorientation of the dipolar moments then takes place in this domain of temperature. The electrical properties concerned with this structural rearrangement are as following: (1) the progressive depolarization ($P_S = f(T)$) of the ceramic characterized by the existence of a depolarization tail [16,17] as schematically represented in the left part of Figure 12, (2) the appearance of a double loop in the hysteresis cycle,[11–13] and (3) the frequency dependent hump of the permittivity.[15]

So, in this temperature range, NBT presents both an antiferroelectric behavior attested by the double loop of the hysteresis cycle and a spontaneous polarization (ferroelectric

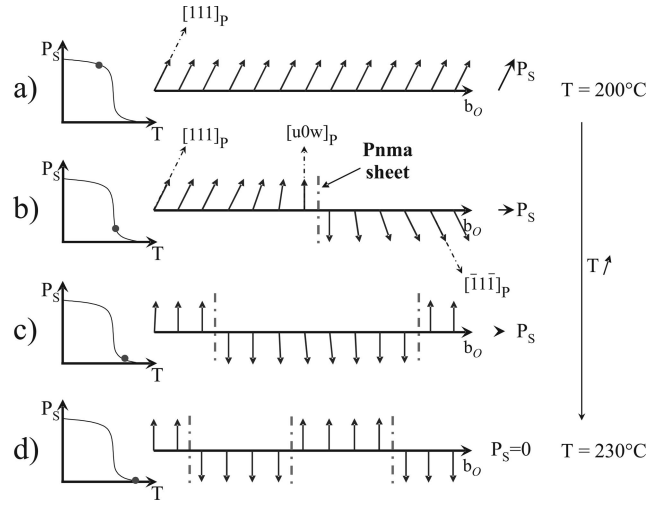

Figure 12. Schematic representation explaining the reorientation of the polar moments as the temperature increases and its influence on the polar character of the crystal which is represented on the left side of the figure ($P_S = f(T)$). (a) At low temperature the crystal presents a *R*3*c* structure in which the cationic displacement occurs along $[111]_P$. In this ideal *R*3*c* crystal, all the $[111]_P$ polar vectors are orientated in the same direction through the crystal, and then $\sum\mu_{\parallel} \neq 0$ and $\sum\mu_{\perp} \neq 0$: the crystal exhibits strong polar character. (b) At higher temperature some *Pnma* sheets appear. Due to the twinning law, the $[111]_P$ polar vectors change to $[\bar{1}\bar{1}\bar{1}]_P$ on the other side of the twin plane. The polar character is then highly reduced. In addition, in areas of the rhombohedral blocks situated in the vicinity of the *Pnma* sheets, the moments are reorientated under the influence of the $[u0w]_P$ polar vectors characteristic of the *Pnma* sheet. The crystal is still polar and ferroelectric but becomes antiferroelectric. (c and d) There are more and more *Pnma* perovskite sheets. The thickness of the *R*3*c* blocks decreases. The overall polar vectors are reorientated along the $[u0w]_P$ directions. The component along the orthorhombic b_O direction of the modulation gradually decreases (polarization tail) until becoming zero ($P_S = 0$), and the crystal is now strictly antiferroelectric.

character) shown by the pyroelectric measurements. This dual property is a peculiar feature case, as usually an antiferroelectric compound is intrinsically not polar.[34] To explain this peculiar behavior, we suggest in a first approach that the formation of the *Pnma* perovskite sheets may involve the reorientation of the polar vectors within the *R*3*c* blocks. Within the perovskite sheets characterized by $a^-a^+a^-$ tilting system leading to the *Pnma* space group, the cationic displacement is necessarily normal to b_O,[35,36] that is, along $[u0w]_P$ directions. The polar vectors, initially orientated along $[111]_P$ in the *R*3*c* blocks, may then be reorientated, at least in the close neighborhood of the *Pnma* sheets. As the temperature increases, the amount of perovskite sheets raises (Figure 10), and their influence on the *R*3*c* blocks becomes stronger. Then at 230 °C, that is, when $P_S = 0$,[16,17] the overall cations are displaced along $[u0w]_P$. Just before the disappearance of the modulated phase, so just below 300 °C the density of orthorhombic sheets is maximum, and according to previous studies, it may correspond to the "isotropization" optical point (~290 °C[9,18,19]) and DSC thermal anomaly (300 °C).[8]

Starting from this model, the dual character that reconciles the ferroelectric and antiferroelectric properties is explained by the respective thickness of the *R*3*c* blocks and the

(34) Lines, M. E.; Glass, A. M. *Principles and applications of ferroelectrics and related materials*; Clarendon Press: Oxford, 2001.
(35) Ali, R.; Yashima, M. *J. Solid State Chem.* **2005**, *178*, 2867–2872.
(36) Kay, H. F.; Bailey, P. C. *Acta Crystallogr.* **1957**, *10*, 219.

correlated number of *Pnma* sheets. At low temperature, there are few *Pnma* sheets and the average thickness of the *R*3*c* blocks is high. In the central part of the blocks, the atomic displacement of cations along $[111]_P$ is maintained and the component along b_O is not zero (Figure 12b). The polar character is partly preserved. The polar property is then always relevant to the rhombohedral phase, while the antiferroelectric property is involved by the microtwinning process. When the temperature increases, the number of *Pnma* sheets raises, and then the thickness of the *R*3*c* blocks decreases. The component along $[111]_P$ decreases, and correlatively the $[u0w]_P$ direction became predominant. The temperature of depolarization is about 230 °C[16,17] [see also Figure 11d], and above this temperature only the antiferroelectric behavior is observed until 280−300 °C.[11–13] If the polarization tail in the PMN relaxor was interpreted by the persistence of polar nanoregions (PNR) in a nonpolar matrix,[37,38] in NBT the polarization tail is due to the progressive reorientation of the polar moment in the *R*3*c* blocks of the modulated phase.

Strictly speaking, the notion of progressive reorientation is somewhat formal. In fact, an arbitrary orientation only represents an average position of cations. Actually, it is more probable that there are solely two possible cationic positions within the polyhedra for both A and B cations, involving two possible displacements based on (1) a displacement along $[111]_P$ typical of the rhombohedral cell and (2) a displacement along $[u0w]_P$ typical of the orthorhombic cell.

In a first approach, we have assumed that, during the formation of the *Pnma* sheets of perovskite, the reorientation of the polar vectors in the vicinity of the sheets was static and continuous (Figure 12). However, near the *Pnma* sheets these two possibilities of cationic displacements within the *R*3*c* blocks may be energetically quasi-equivalent. As a consequence a dynamical cationic movement may operate, and the cations may jump between $[111]_P$ and $[u0w]_P$ directions. The actual position of the cations may then fluctuate between these two types of sites, inducing a local change in the orientation of the polar vectors. Statistically, as the thickness of the *R*3*c* blocks decreases, the probability for the $[u0w]_P$ type displacement may increase with the temperature.

In a general rule, the relaxor behavior is due to the change in direction and/or amplitude of the polar vectors. In PMN it was shown that the polar vectors are situated within the PNR which displays rhombohedral symmetry. In this compound the cations jump between eight equivalent positions along the 3-fold axis of the rhombohedral cell giving rise to the so-called relaxor behavior. In NBT, this relaxor property may be linked to the existence of the modulated phase. Indeed, the dynamical character of the cationic jump from one site to another near the interface between the *R*3*c* blocks and the *Pnma* sheets is a possible reason explaining the relaxor behavior of NBT in this temperature range.

Above 230 °C the relaxor behavior is not observed.[14] According to the presented results, the thickness of the *R*3*c* blocks is then limited to six to seven atomic cells (Figure 2), and the polar vectors are then totally reorientated along $[u0w]_P$. The cationic position is definitely established, preventing any relaxor behavior. The same kind of relaxor behavior has been observed in other perovskites which also show a first order reconstructive phase transition relying on the formation of an intermediate modulated phase.[39–42] All these compounds present the same succession in the dielectric anomalies as NBT. The phase transitions in NBT are not a particular feature case.

Conclusion

The in situ TEM analysis performed on NBT by electron diffraction and conventional imaging allows understanding the R → T phase transition.

(1) The destabilization of the *R*3*c* rhombohedral phase, attested by the disappearance of the ferroelectric domains, begins near 200 °C.

(2) A modulated phase develops between 200 and 300 °C. It is formed of *Pnma* orthorhombic sheets, appearing within the *R*3*c* matrix and exhibiting $a^-a^+a^-$ octahedra tilting system. These sheets are in fact twin boundaries between two *R*3*c* ferroelectric domains. As the temperature increases, a microtwining process takes place, generating more and more *Pnma* sheets. The minimization of the strain energy results in a quasi-commensurate character of the modulated phase.

(3) The increasing density of *Pnma* sheets, in which the cations are displaced along $[u0w]_P$, leads to a reorientation of the polar vector within the *R*3*c* perovskite blocks. Thus, due to the pseudomerohedral twining law, two successive ferroelastic−ferroelectric *R*3*c* domains present polar vectors orientated in opposite directions in a plane perpendicular to the modulated direction. The modulated phase explains the antiferroelectric property of NBT in this temperature range.

(3) The modulated phase is also at the origin of the relaxor behavior of NBT. In the close neighborhood of the *Pnma* sheets, the cations may occupy two kinds of atomic positions which are nearly equivalent from the point of view of their energy. These two positions are defined by the local structure of the *R*3*c* blocks and the *Pnma* sheets. The cations could then alternately jump from one position to the other, giving rise to the so-called relaxor behavior of NBT.

CM8004634

(37) Samara, G. A. *Solid State Phys.* **2001**, *56*, 239–458.
(38) Cross, L. E. *Ferroelectrics* **1987**, *76*, 241–267.
(39) Tan, X.; He, H.; Shang, J.-K. *J. Mater. Res.* **2005**, *20* (7), 1641–1653.
(40) Xu, Z.; Viehland, D.; Payne, D. A. *J. Mater. Res.* **1995**, *10* (2), 453–460.
(41) Xu, Z.; Viehland, D.; Yang, P.; Payne, D. A. *J. Appl. Phys.* **1993**, *74* (5), 3406–3413.
(42) Youn, S. C.; Choo, W. K. *J. Eur. Ceram. Soc.* **2004**, *24*, 1497–1500.